Int. J. Solids Structures Vol. 26, No. 8, pp. 851–864, 1990
Printed in Great Britain.

0020-7683/90 $3.00 + .00

TWO-DIMENSIONAL TRANSIENT WAVE-PROPAGATION PROBLEMS BY TIME-DOMAIN BEM

A. S. M. ISRAIL and P. K. BANERJEE
Department of Civil Engineering, State University of New York at Buffalo, 212 Ketter Hall, Buffalo, NY 14260, U.S.A.

(*Received* 7 *July* 1989; *in revised form* 12 *October* 1989)

Abstract—In this paper, an advanced formulation of time-domain Boundary Element Method (BEM) for linear elastodynamics is used to study a number of problems involving wave propagation through half-space as well as multi-layered soils. The algorithm incorporates isoparametric quadratic elements which facilitate proper modelling of problem geometry and can represent the field variables in dynamic problems very accurately, which are very often wavy in nature. Also higher order temporal variation of functions is introduced. Improved techniques are employed for the accurate evaluation of both the singular and non-singular spatial integrals. Most importantly, this formulation incorporates simpler and better behaved kernels compared to those that have appeared in the recent BEM literature by the present and other previous researchers. With all these new and efficient features the present formulation is superior to the existing ones and as such represents a very effective tool for solving 2D transient wave propagation problems, especially in infinite and semi-infinite domains where other numerical methods have considerable difficulty in producing accurate solutions.

INTRODUCTION

Propagation of elastic waves through half-space or layered half-space is of considerable interest to engineers, geologists and seismologists. Lacking any analytical method to treat such problems, resort has been made to various numerical techniques such as the Finite Element Method (FEM), Boundary Element Method (BEM) etc. The Finite Element Method is generally very effective for problems with complex geometries and material properties. However, it has a disadvantage when the problem involves a semi-infinite or infinite domain because of its difficulty in modelling such domains. The Boundary Element Method, on the other hand, with its inherent ability to satisfy the radiation condition, does not need modelling of the far field and as such is extremely suitable for this class of problems. Besides, the reduction of problem dimensionality and overall increased numerical accuracy (Banerjee and Butterfield, 1981) are the other advantages.

Most of the earlier work on transient wave propagation by BEM involved transform domain formulations in conjunction with a numerical inversion scheme. For example, Cruse and Rizzo (1968) studied two-dimensional problems of elastic half-plane under transient load, Niwa *et al.* (1975) solved the problem of transient wave scattering by cavities of arbitrary shapes due to the passage of travelling waves, and recently, Ahmad and Banerjee (1988) investigated a number of 2D wave-propagation problems using an advanced algorithm of Laplace-domain transient BEM.

Direct time-domain BEM formulation for 2D transient dynamic problems started only recently with the works of Mansur (1983) and Antes (1985). However, the accuracy of their formulation suffers from the following: mathematical complexity resulting from the treatment of Heaviside functions present in the kernel functions, simplified assumptions of constant variation of spatial variables, modelling of boundary geometry by using straight line segments, inadequate treatment of edges and corners, etc. Nevertheless, these are pioneering first-generation BEM implementation in 2D transient dynamics.

The approach of modelling the boundary geometry by straight line segments and assuming the field variables to be constant within a segment may be justified for very simple problems. But for real problems with corners and edges and/or curvilinear geometry, higher order elements are needed for proper modelling. Moreover, for dynamic problems, where field variables are usually wavy in nature, higher order variation of the field quantities needs to be incorporated for accurate results.

The present algorithm offers a simplified formulation for time-domain BEM together with isoparametric quadratic elements. This implementation has the capability of solving problems with multiple modelling regions (up to 15). The singular integral involving the traction kernel is evaluated using a rigid body technique incorporating the corresponding elastostatic kernel. The singular and non-singular integrals are evaluated using a scheme with intelligent subsegmentation and optimum Gauss points which seem to improve numerical accuracy. Additionally, some of the terms in the convoluted boundary kernels have been transformed to reduce the apparent singularity at the wave front and are improvements over the earlier work of Israil and Banerjee (1989).

As stated earlier, a number of wave propagation problems have been studied. These involve generation of Rayleigh waves in an elastic half-space, Love waves in layered soil, vibration isolation using open and infilled trenches, and surface disturbances due to an underground explosion in a multi-layered soil. Each of these problems studied has considerable practical significance. Moreover, there are few numerical methods capable of solving this type of problem involving semi-infinite domains with sufficient accuracy. For example, it is well known that it is difficult to show Rayleigh waves in an elastic half-plane using any numerical method. Demonstration of the ability to solve a class of such complex wave propagation problems is the essence of this paper.

TIME-DOMAIN BEM FORMULATION

The time-domain boundary integral equation can be derived by combining the fundamental point-force solution of the governing differential equation of motion with the actual solution state via the use of Graffi's (1947) dynamic reciprocal theorem and is as follows:

$$c_{ij}(\xi)u_i(\xi, T) = \int_S \int_0^T [G_{ij}(\mathbf{x}, T; \xi, \tau)t_i(\mathbf{x}, \tau) - F_{ij}(\mathbf{x}, T; \xi, \tau)u_i(\mathbf{x}, \tau)]\, d\tau\, dS(\mathbf{x}) \qquad (1)$$

where $G_{ij}(\mathbf{x}, T; \xi, \tau)$ is Stokes' solution in 2D and represents the displacements at a point x at time T due to a unit point force applied at ξ at a preceding time τ. It has the following properties:

(i) causality: $G_{ij}(\mathbf{x}, T; \xi, \tau) = 0$ where $c_2(T-\tau) < |\mathbf{x}-\xi|$, i.e. the contribution due to each type of wave is null if the wave has not reached the field point;
(ii) reciprocity: $G_{ij}(\mathbf{x}, T; \xi, \tau) = G_{ij}(\xi, -\tau; \mathbf{x}, -T)$;
(iii) time-translation: $G_{ij}(\mathbf{x}, T+t_1; \xi, \tau+t_1) = G_{ij}(\mathbf{x}, T; \xi, \tau)$;
(iv) symmetry: $G_{ij}(\mathbf{x}, T; \xi, \tau) = G_{ji}(\mathbf{x}, T; \zeta, \tau)$.

$F_{ij}(\mathbf{x}, T; \xi, \tau)$ is the traction kernel obtained from the G_{ij} kernel through the proper mathematical process by taking care of the causality of the waves (Israil and Banerjee, 1989) and is different from and simpler than those obtained by Mansur (1983).

$c_{ij}(\xi)$ is the well-known discontinuity term and assumes the following values:

(i) δ_{ij} for ξ within the volume V of the body;
(ii) $0.5\delta_{ij}$ for ξ on a smooth surface S; and
(iii) 0 for ξ outside the volume V and surface S.

In eqn (1), contributions due to the initial conditions are neglected. In this implicit time-domain formulation, the response at time T is obtained by taking into account the history of the field variables up to and including time T.

NUMERICAL IMPLEMENTATION

For numerical implementation of eqn (1), discretizations in both time and space are required. The temporal functions are simple enough to carry out the time integrations

analytically while the spatial integrations are to be treated numerically. The salient features of the temporal and spatial integrations are outlined below.

(a) *Temporal integration*

The time axis is divided into N equal steps so that $T = N\Delta T$. Both linear and mixed (described later) temporal variations of the functions are incorporated.

(i) *Linear variation.* The field variables are assumed to vary linearly during a time step and can be expressed as:

$$f_i(\mathbf{x},\tau) = M_1(\tau) f_i^n(\mathbf{x}) + M_2(\tau) f_i^{n-1}(\mathbf{x}) \tag{2}$$

where $f_i(\mathbf{x},\tau)$ stands for tractions or displacements and $M_1(\tau)$ and $M_2(\tau)$ are linear temporal shape functions, given by:

$$M_1(\tau) = \frac{\tau - T_{n-1}}{\Delta T}, \quad M_2(\tau) = \frac{T_n - \tau}{\Delta T}; \quad T_{n-1} < \tau < T_n,$$

where the subscripts 1 and 2 refer to the forward and backward temporal nodes, respectively, during a time step.

With the linear variation of functions described above, eqn (1) takes the form:

$$c_{ij}(\xi) u_i^N(\xi) = \sum_{n=1}^{N} \int_S \left([G_{ij_1}^{N-n+1} + G_{ij_2}^{N-n}] t_i^n(\mathbf{x}) - [F_{ij_1}^{N-n+1} + F_{ij_2}^{N-n}] u_i^n(\mathbf{x}) \right) \mathrm{d}S(\mathbf{x}) \tag{3}$$

where $G_{ij_1}^{N-n+1}$, $F_{ij_1}^{N-n+1}$ etc. are the convoluted kernels which can be found in Israil and Banerjee (1989).

In evaluating the convoluted G_{ij} and F_{ij} kernels, the computational effort can be greatly reduced by making use of the time-translation property of the kernels. That is, at each time step only the effect of the dynamic history of the first time interval on the current time node needs to be evaluated, i.e. at each time step, the analytical time integration has to be carried only for $n = 1$. However, the convoluted F_{ij} kernels contain terms that sometimes cause difficulty in numerical integration especially for a mesh with widely varying element lengths. But, when kernels are combined as shown in eqn (3), those terms cancel each other and result in well-behaved functions. This new form of the kernels is presented below:

$$\begin{aligned}
G_{ij_1}^N + G_{ij_2}^{N-1} = \frac{1}{2\pi\rho} \sum_{m=1}^{2} \frac{1}{c_m^2} \Bigg[& \frac{\delta_{ij}}{2} \Bigg[N \cosh^{-1}\left(\frac{c_m N \Delta T}{r}\right) - 2(N-1)\cosh^{-1}\left\{\frac{c_m (N-1)\Delta T}{r}\right\} \\
& + (N-2)\cosh^{-1}\left\{\frac{c_m (N-2)\Delta T}{r}\right\} \Bigg] + (-1)^m \tfrac{1}{2}(\delta_{ij} - 2r_{,i}r_{,j}) \left(\frac{c_m \Delta T}{r}\right)^2 \Bigg[N^2 \sqrt{N^2 - \left(\frac{r}{c_m \Delta T}\right)^2} \\
& - 2(N-1)^2 \sqrt{(N-1)^2 - \left(\frac{r}{c_m \Delta T}\right)^2} + (N-2)^2 \sqrt{(N-2)^2 - \left(\frac{r}{c_m \Delta T}\right)^2} \Bigg] \\
& - (-1)^m \tfrac{1}{3}(\delta_{ij} - 2r_{,i}r_{,j}) \Bigg[\left\{ N^2 - \left(\frac{r}{c_m \Delta T}\right)^2 \right\}^{3/2} - 2\left\{ (N-1)^2 - \left(\frac{r}{c_m \Delta T}\right)^2 \right\}^{3/2} \\
& + \left\{ (N-2)^2 - \left(\frac{r}{c_m \Delta T}\right)^2 \right\}^{3/2} \Bigg] - (-1)^m (\delta_{ij}\delta_{2m} - r_{,i}r_{,j}) \Bigg[\sqrt{N^2 - \left(\frac{r}{c_m \Delta T}\right)^2} \\
& - 2\sqrt{(N-1)^2 - \left(\frac{r}{c_m \Delta T}\right)^2} + \sqrt{(N-2)^2 - \left(\frac{r}{c_m \Delta T}\right)^2} \Bigg] \Bigg]
\end{aligned} \tag{4}$$

$$F^N_{ij_1}+F^{N-1}_{ij_2}=\frac{\mu}{2\pi\rho r}\sum_{m=1}^{2}\left[\left\{\frac{-A_1\delta_{1m}+A_3\delta_{2m}}{c_m^2}\right\}\left[\sqrt{N^2-\left(\frac{r}{c_m\Delta T}\right)^2}-2\sqrt{(N-1)^2-\left(\frac{r}{c_m\Delta T}\right)^2}\right.\right.$$
$$\left.+\sqrt{(N-2)^2-\left(\frac{r}{c_m\Delta T}\right)^2}\right]-(-1)^m A_2\left(\frac{\Delta T}{r}\right)^2\left[\left\{N^2-\left(\frac{r}{c_m\Delta T}\right)^2\right\}^{3/2}\right.$$
$$\left.\left.-2\left\{(N-1)^2-\left(\frac{r}{c_m\Delta T}\right)^2\right\}^{3/2}+\left\{(N-2)^2-\left(\frac{r}{c_m\Delta T}\right)^2\right\}^{3/2}\right]\right] \quad (5)$$

where

$$A_1=\frac{\lambda}{\mu}n_i r_{,j}+2r_{,i}r_{,j}\frac{\partial r}{\partial n}$$

$$A_2=n_i r_{,j}+n_j r_{,j}+\frac{\partial r}{\partial n}(\delta_{ij}-4r_{,j}r_{,j})$$

$$A_3=\frac{\partial r}{\partial n}(2r_{,i}r_{,j}-\delta_{ij})-n_j r_{,i}.$$

In expressions (4) and (5) the time-related terms are always non-negative because of the causality property of the waves.

These expressions also reduce to the corresponding elastostatic kernels at a large time step. The pertinent algebra is similar to that shown in Israil and Banerjee (1989).

(ii) *Mixed variation.* For problems where the traction boundary condition is applied as a sudden jump, a mixed kind of variation produces better results. In this formulation, the traction is assumed to remain constant while the displacement is taken to be linear during a time step. Thus, the G_{ij} and F_{ij} kernels are the same as those corresponding to constant and linear variation, respectively. However, for the sake of convenience of housekeeping one-half of the time-convoluted G_{ij} kernel is assigned to each of the two local time nodes and after proper condensation the expression corresponding to eqn (4) is:

$$G^N_{ij_1}+G^{N-1}_{ij_2}=\frac{1}{4\pi\rho}\sum_{m=1}^{2}\frac{1}{c_m^2}\left[\frac{\delta_{ij}}{2}\left[\cosh^{-1}\left(\frac{c_m N\Delta T}{r}\right)-\cosh^{-1}\left\{\frac{c_m(N-2)\Delta T}{r}\right\}\right]\right.$$
$$+(-1)^m\tfrac{1}{2}(\delta_{ij}-2r_{,i}r_{,j})\left(\frac{c_m\Delta T}{r}\right)^2\left[N\sqrt{N^2-\left(\frac{r}{c_m\Delta T}\right)^2}\right.$$
$$\left.\left.-(N-2)\sqrt{(N-2)^2-\left(\frac{r}{c_m\Delta T}\right)^2}\right]\right]. \quad (6)$$

The convoluted F_{ij} kernels are the same as given by (5). The rest of the time-stepping scheme is similar to the linear formulation.

(b) *Spatial integration*

(i) *Representation of geometry and functions.* Using isoparametric quadratic elements, the coordinates and the functions (displacements and tractions) at any point over an element can be expressed in terms of the nodal values as:

$$x_i=N_\alpha(\eta)X_{i\alpha}$$
$$u_i=N_\alpha(\eta)U_{i\alpha}$$

$$t_i = N_\alpha(\eta) T_{i\alpha}$$

where

$i = 1, 2$ for 2D

$\alpha = 1, 2, 3$ for a quadratic element

and

$N_\alpha(\eta)$ are the shape functions in the intrinsic coordinates (η) of the element.

(ii) *Discretized form of BEM equation.* After the spatial discretization process described above, eqn (3) is transformed into:

$$c_{ij}(\xi) u_i^N(\xi) = \sum_{n=1}^{N} \sum_{m=1}^{M} \left[\sum_{\alpha=1}^{3} T_{i\alpha}^n \int_0^1 [G_{ij_1}^{N-n+1} + G_{ij_2}^{N-n}] N_\alpha(\eta) |J| \, d\eta - \sum_{\alpha=1}^{3} U_{i\alpha}^n \int_0^1 [F_{ij_1}^{N-n+1} + F_{ij_2}^{N-n}] N_\alpha(\eta) |J| \, d\eta \right] \quad (7)$$

where M is the total number of boundary elements and $|J|$ is the Jacobian of the transformation.

(iii) *Evaluation of the singular integrals.* The integral involving F_{ij_1} kernels has the same type and order of singularity as the corresponding elastostatic kernel during the first time step and it is evaluated in the following way:

$$D_{ij} = c_{ij} + \int_{S_1} F_{ij_1}^{\text{trans}} N_1 \, dS \quad (8)$$

where c_{ij} is the jump term, N_1 is the shape function at the singular node and S_1 is the length of the singular element. The integral is the Cauchy Principal Value (CPV).

Similarly, for a static problem,

$$D_{ij}^S = c_{ij} + \int_{S_1} F_{ij}^{\text{static}} N_1 \, dS. \quad (9)$$

From eqns (8) and (9), one can write:

$$D_{ij} = D_{ij}^S + \int_{S_1} (F_{ij_1}^{\text{trans}} - F_{ij}^{\text{static}}) N_1 \, dS. \quad (10)$$

D_{ij}^S can be evaluated using the well-known technique of rigid body motions, i.e.

$$D_{ij}^S = -\left[\sum_{\alpha=2}^{3} \int_{S_1} F_{ij}^{\text{static}} N_\alpha \, dS + \sum_{m=2}^{M} \sum_{\alpha=1}^{3} \int_{S_1} F_{ij}^{\text{static}} N_\alpha \, dS \right]. \quad (11)$$

The second integral in eqn (10) is non-singular and hence D_{ij} can be determined from that equation without much difficulty.

It should be mentioned here that for the evaluation of D_{ij}^S from eqn (11), the body must have a closed boundary. Thus for half-plane problems, the region of interest must be enclosed with fictitious boundary elements known as "enclosing elements". For a detailed discussion, interested readers are referred to the paper by Ahmad and Banerjee (1988).

The singularity of the transient G_{ij_1} kernel is a weak one and hence its numerical evaluation does not pose any special difficulty. In general, the spatial variation of the kernels is not smooth and hence an integration scheme using intelligent subsegmentations and optimum Gauss points per subsegment is employed for accurate evaluation of both the singular and non-singular integrals.

(iv) *Multi-region.* One of the important features of the present algorithm is its ability to solve problems with multiply-connected regions. This is accomplished by formulating the BEM system of equations for each region independently and then assembling them together by satisfying equilibrium of tractions and compatibility of displacements across the common interfaces. Because these equations satisfy the governing differential equation for each region there is no residual kinetic energy imbalance at these interfaces. This multi-region implementation can at present handle problems with up to 15 modelling regions.

(v) *Solution procedure.* Equation (7) can be written sequentially for each of the boundary nodes and once both temporal and spatial integration are complete can be put into the following matrix form:

$$\sum_{n=1}^{N} [[G_1^{N-n+1} + G_2^{N-n}]\{t^n\} - [F_1^{N-n+1} + F_2^{N-n}]\{u^n\}] = \{0\} \tag{12}$$

where $\{t^n\}$, $\{u^n\}$ etc. are the vectors of nodal tractions and displacements, respectively, with the superscript referring to the global time node index.

At time T, only half the boundary variables are unknown, the rest are known and so is the past history. Equation (12) then can be rearranged to:

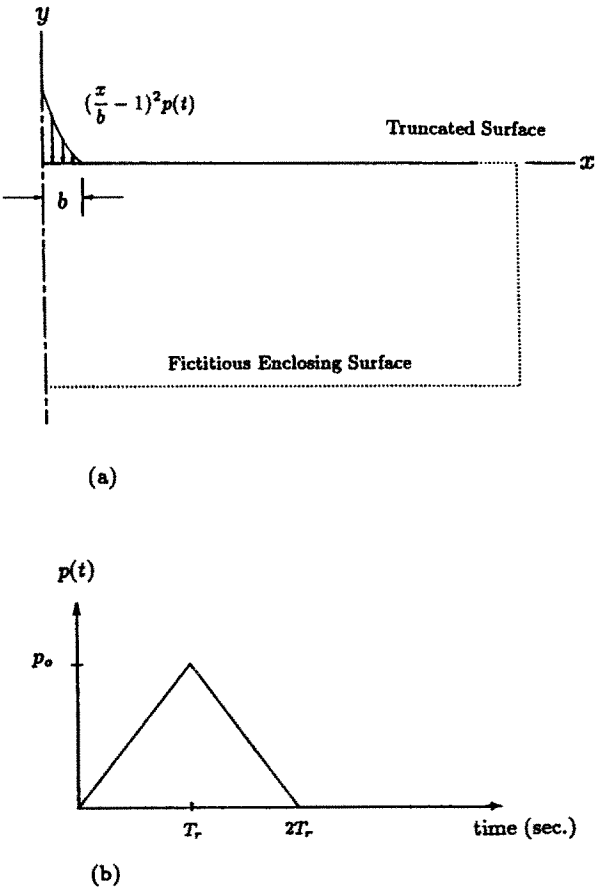

Fig. 1. (a) Parabolic load on half-space. (b) Time history of the applied load.

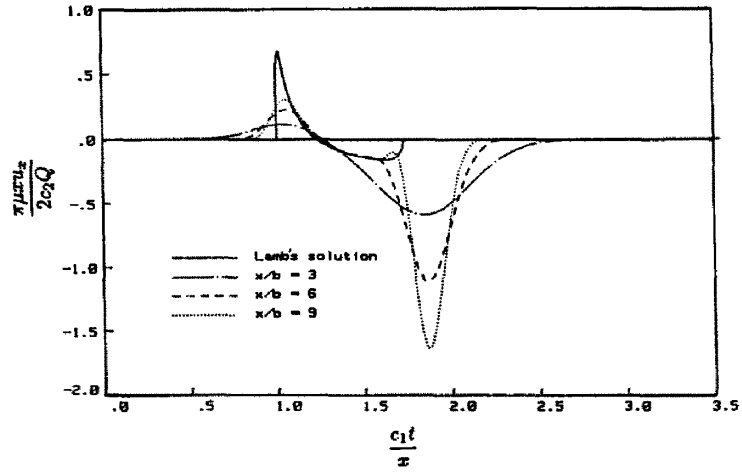

(a)

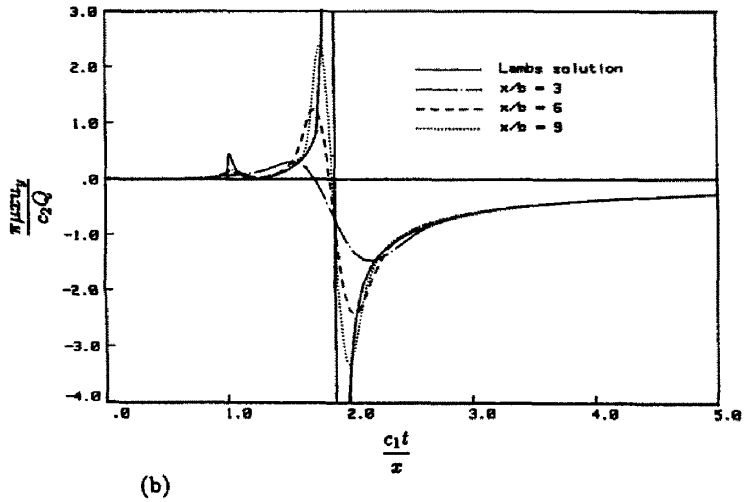

(b)

Fig. 2. Displacements at the surface of loaded half-space. (a) Horizontal displacement. (b) Vertical displacement.

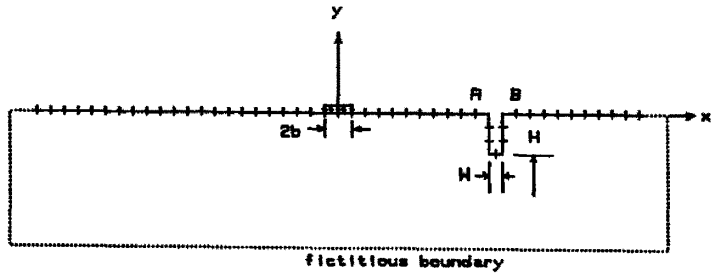

Fig. 3. Discretization pattern of a loaded half-space with trench.

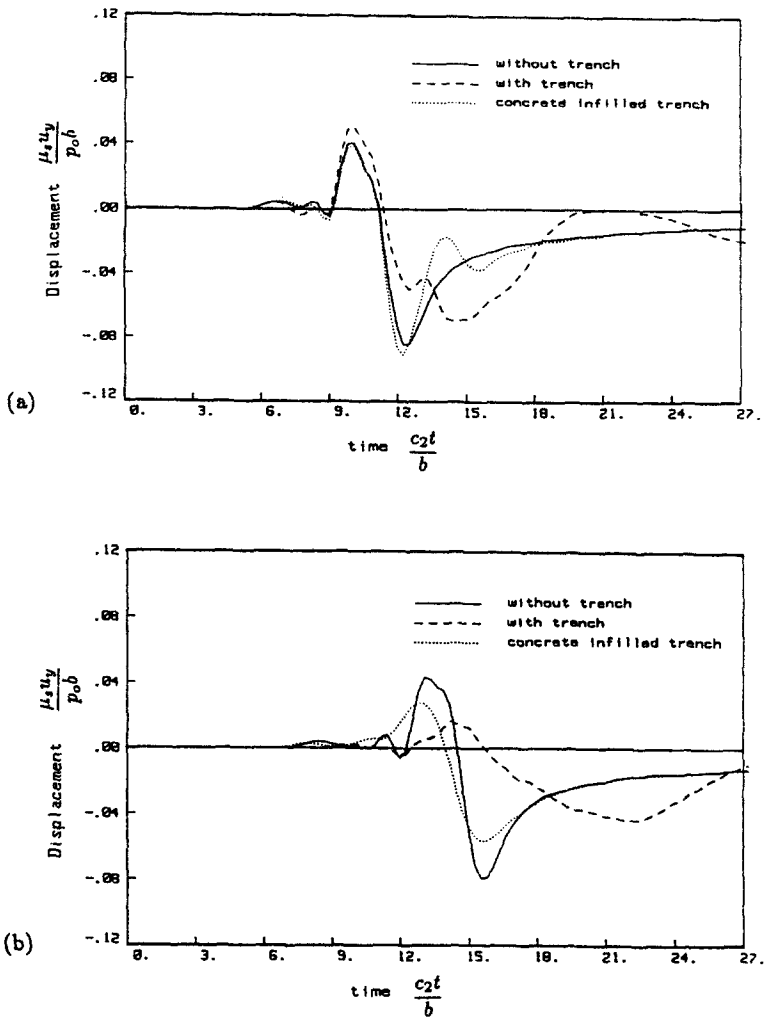

Fig. 4. Effect of open trench vs concrete-infilled trench on transient vibration. (a) Point A. (b) Point B.

$$[A_1^1]\{X^N\} = [B_1^1]\{Y^N\} - \sum_{n=1}^{N-1}([G_1^{N-n+1} + G_2^{N-n}]\{t^n\} - [F_1^{N-n+1} + F_2^{N-n}]\{u^n\})$$

or

$$[A_1^1]\{X^N\} = [B_1^1]\{Y^N\} + \{R^N\} \tag{13}$$

in which $\{X^N\}$ and $\{Y^N\}$ are the vectors of the unknown and known quantities at time T and $\{R^N\}$ represents the effect of past dynamic history on the current time node.

Equation (13) can be solved for the unknown boundary values using any standard solution procedure.

APPLICATIONS

The results obtained from a series of studies on two-dimensional wave propagation are presented here with each problem designed to demonstrate a specific aspect. Those include the ability of this algorithm to show Rayleigh wave generation in an elastic half-plane, generation of Love waves in layered soils. transient vibration–isolation in a half-plane and the study of surface disturbances due to an underground explosion in a multi-layered soil.

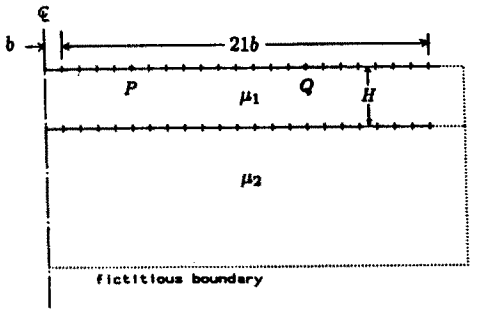

(a)

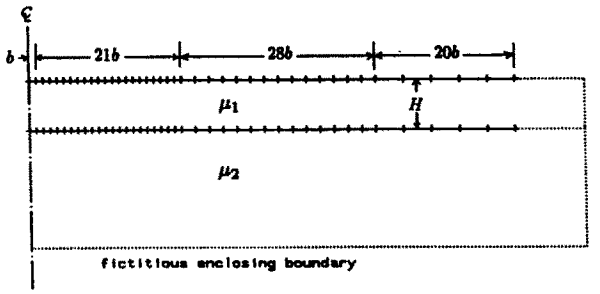

(b)

Fig. 5. Discretization of layered half-space. (a) Truncated discretization (mesh 1). (b) Extended discretization (mesh 2).

Since the formulation has the capability of taking advantage of symmetry in load and geometry, this facility was exploited wherever possible in reducing the computational time and effort. Most of the solutions are presented in a normalized form. In case of layered media, parameters corresponding to the upper layer were used for normalization unless otherwise mentioned.

(a) *Surface displacements of a loaded half-space*

This example illustrates the generation of Rayleigh waves in a loaded half-plane, which is known to be very difficult by any numerical method.

The analytical treatment of the problem was given by Lamb (1904). He presented the complete solution for the vertical surface displacement but for horizontal displacement, results were given only till the arrival of the *S*-wave, missing out the very important Rayleigh wave component. Numerical treatment of this problem does not appear to exist in the published literature.

The elastic half-space shown in Fig. 1a is loaded with a stress field, the spatial variation of which is parabolic and the temporal variation is in the form of a triangular pulse (Fig. 1b). The parabolic spatial distribution is chosen to simulate a point load (line load, in 2D) while the triangular pulse was taken to simulate a delta pulse in time. Because of spatial symmetry, only one-half of the problem geometry is modelled using 44 quadratic elements.

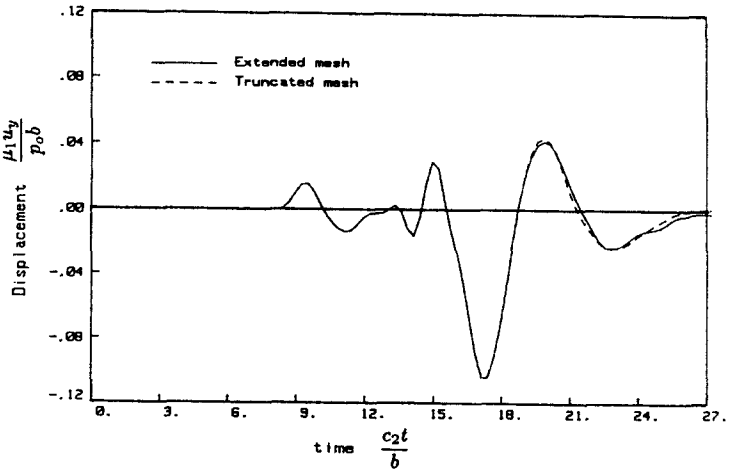

(a)

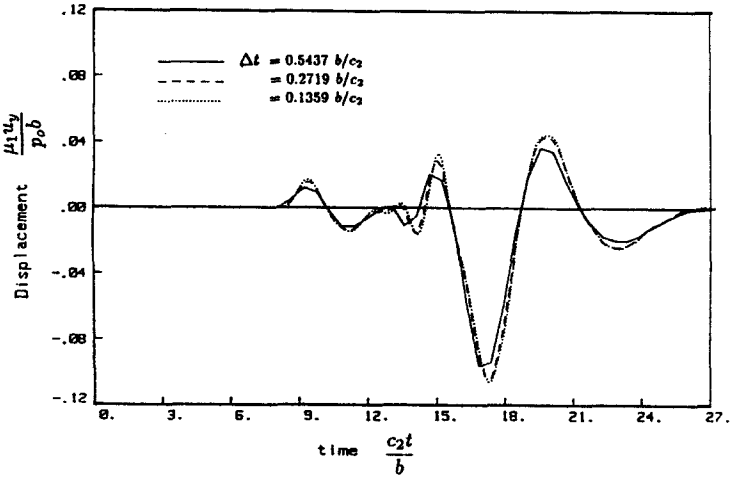

(b)

Fig. 6. (a) Effect of truncation on vertical displacement at point Q ($x/b = 15$). (b) Effect of time step on vertical displacement at the same location.

The discretization is extended up to a distance of $22b$, where b is the half-width of the loaded region. The time step is chosen such that during one step the P-wave travels over one-half of the element.

The surface displacements obtained by the present formulation at different locations are presented in Fig. 2. The normalization parameters are: x, the distance of the point from the center of the loaded region; μ, the shear modulus; c_1 and c_2, the propagational velocities of the P- and S-wave, respectively; and Q, the magnitude of the triangular pulse (area under the curve in Fig. 1b). Notice that as the point is farther away from the loaded region the results converge towards Lamb's solution indicating that with increasing distance the load appears to be a point load.

(b) *Vibration isolation with open and infilled trench*

Vibration due to transient loads can be reduced by the use of a trench. In this study, the effectiveness of an open trench as opposed to a concrete-infilled trench in attenuating the amplitude of transient vibration is investigated.

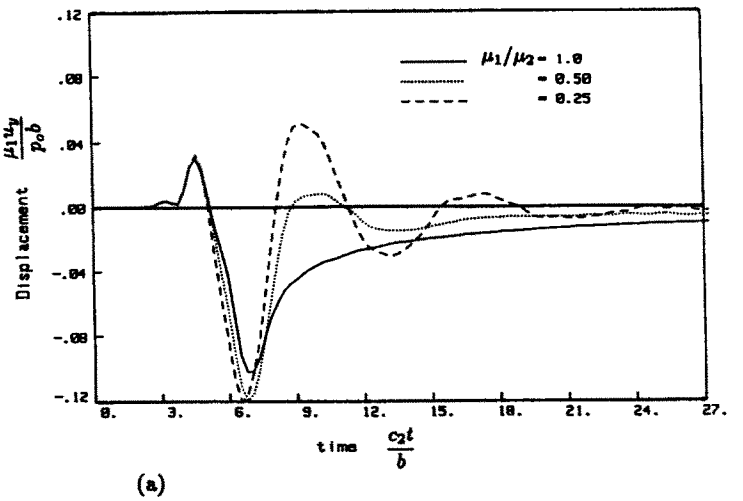

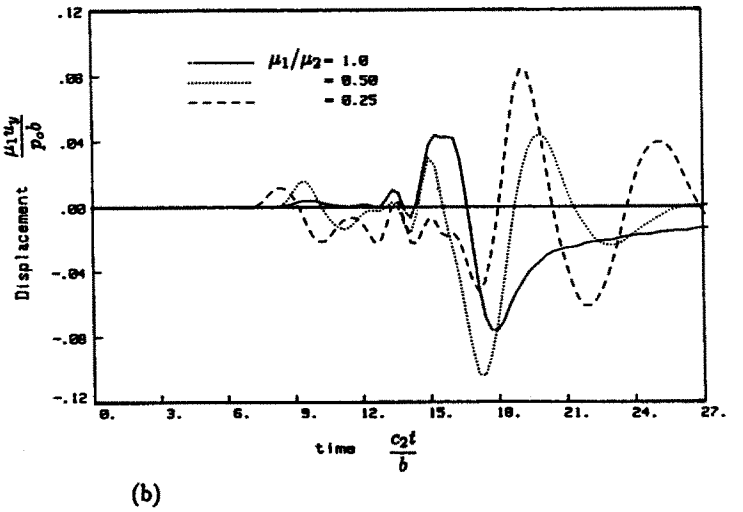

Fig. 7. (a) Effect of shear moduli of the layers (μ_1/μ_2) on the vertical displacement. (b) Point P ($x/b = 5$). (b) Point Q ($x/b = 15$).

The discretization pattern of the problem is shown in Fig. 3a. The portion of the half-space of width $2b$ is subjected to a uniform stress, the time history of which is the same as in Fig. 1b. The rise-time of the load is $T_r = 0.5437b/c_2$. A trench of width $W = b$ and depth $H = 3b$ is located at a distance of $10b$ from the edge of the loaded portion. The vertical displacements at points $A(10b, 0)$ and $B(13b, 0)$ located before and after the trench, respectively, are of interest here. The material properties of the soil medium and concrete are:

$$\mu_c/\mu_s = 34.29; \quad \nu_s = \nu_c = 0.25; \quad \rho_c/\rho_s = 1.37.$$

The results obtained using no trench, an open trench and a concrete-infilled trench are presented in Fig. 4. For point A, the presence of a concrete-infilled trench made no significant difference to the response as compared to no trench. The presence of an open trench increased the duration of high-amplitude vibration, probably due to reflection from the trench wall. However, for point B, the open trench helped to attenuate the amplitude of vibration significantly, while the concrete-infilled trench reduced the vibration to some

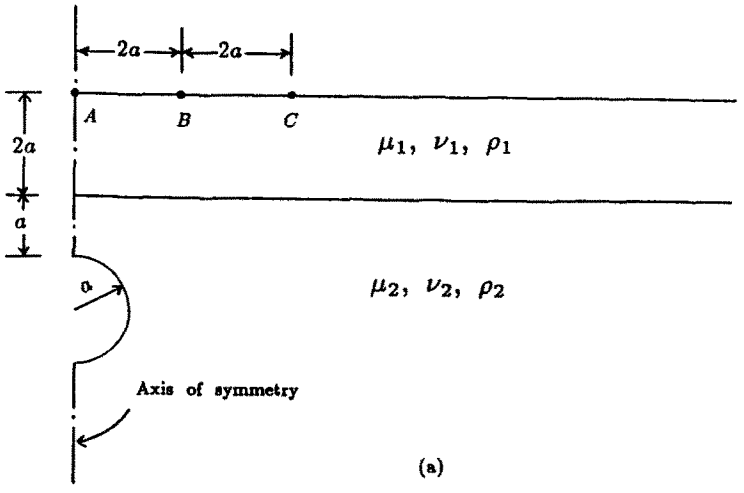

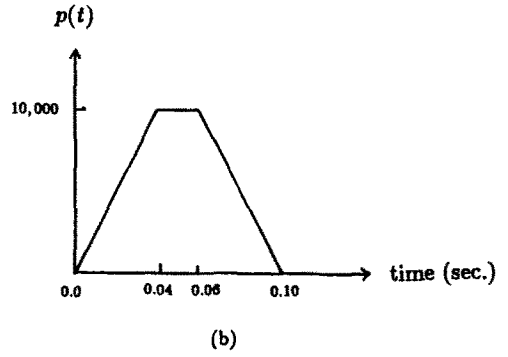

Fig. 8. (a) Underground explosion in a two-layered soil. (b) Time history of applied internal radial pressure on the cavity wall.

extent. Note that the arrival of the *P*-wave is delayed in the case of an open trench while it arrives early in the case of an infilled trench because the wave travels faster through concrete.

These results show that an open-trench is more effective in reducing transient vibration than a concrete-infilled trench, at least in this example.

(c) *Wave propagation through layered soil*

In the real world, the soil profile is almost never a homogeneous half-space. In many instances, it is stratified with softer layers overlying the stiffer ones. The presence of such layers affects the wave propagation significantly. Waves emanating from the loaded surface undergo reflection and refraction at the interface between the layers and give rise to new types of waves such as Love waves, etc.

The present study involves a loaded two-layered soil profile as shown in Fig. 5 with different shear moduli μ_1 and μ_2, all other properties remaining the same in the two layers. The depth of the upper layer is $H = 3b$. The portion of the top surface of width $2b$ is loaded with the triangular pulse of Fig. 1b. The rise time of the pulse is $T_r = 0.5437b/c_2$, where c_2 is the shear-wave velocity in the upper layer. Because of symmetry, only one-half of the problem is modelled.

The effect of a truncated mesh on the surface displacements was studied using two types of mesh pattern: one extended up to a distance of $22b$ (mesh 1) and the other up to $70b$ (mesh 2). Both the meshes are shown in Fig. 5. The study was conducted for a layered profile with $\mu_1/\mu_2 = 0.5$ and a time step of $\Delta t = 0.2719b/c_2$. The effect of truncation on the vertical displacement of a point Q ($x/b = 15$) is depicted in Fig. 6a. The results from the

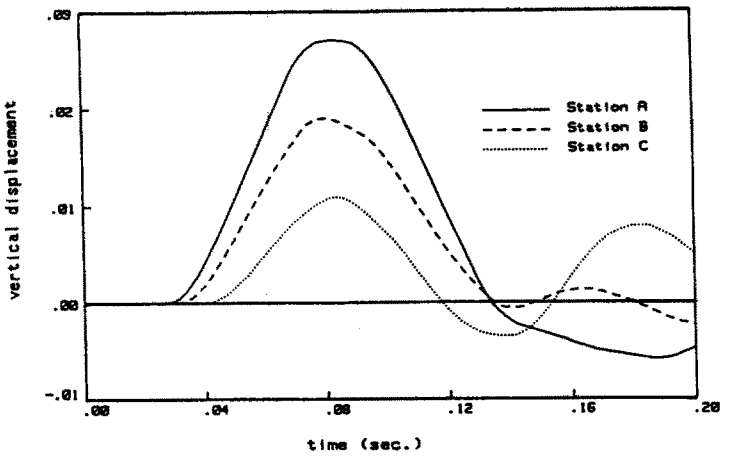

(a)

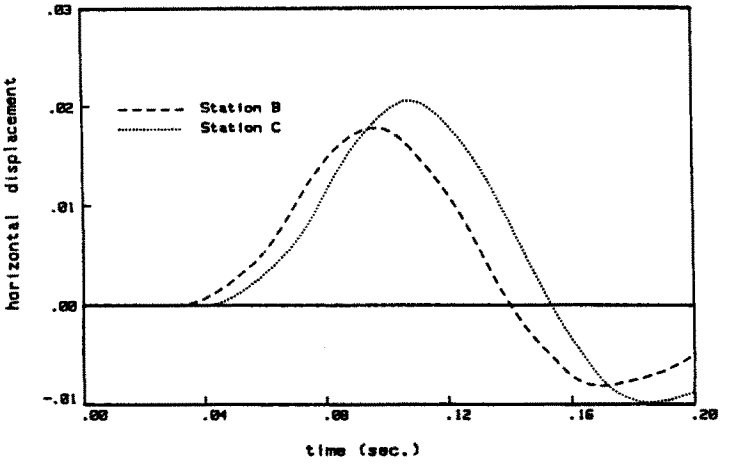

(b)

Fig. 9. Surface disturbances at various locations due to underground explosion. (a) Vertical. (b) Horizontal.

two meshes are identical except for some insignificant differences at later times. For points closer to the loaded region the solutions were identical while noticeable differences were present for points very close to the truncated end. Another study was conducted to investigate the effect of the time step on the vertical response. Mesh 1 was used together with three different time steps: $\Delta t = 0.5437b/c_2$, $\Delta t = 0.2719b/c_2$ and $\Delta t = 0.1359b/c_2$. The results obtained at the same location are presented in Fig. 6b. It is observed that the solutions obtained using the two smaller time steps are almost identical, indicating convergence of the results. Mesh 1 and time step $\Delta t = 0.2719b/c_2$ were chosen for further study.

Three different layered profiles were studied with the ratios of shear moduli: $\mu_1/\mu_2 = 1.0$, 0.5 and 0.25. The vertical displacements at the locations P ($x/b = 5$) and Q ($x/b = 15$) are presented in Fig. 7. As the bottom layer becomes stiffer, more waves are reflected from the interface and generate Love waves in the top layer, and thus the surface displacement become oscillatory. Moreover, waves travel faster through the lower stiffer medium and arrive early at a given point as compared to when the medium is softer. This phenomenon is pronounced for distant points as can be seen in Fig. 7b.

(d) *Underground explosion in a layered soil medium*

The disturbance of the soil surface due to an underground explosion is studied in this example.

The soil profile is assumed to consist of a layered stratum overlaying a half-space. The explosion is simulated via a sudden radial expansion of a cylindrical cavity in the underlying half-space. The soil profile with the various dimensions and the time history of the applied pressure in the cavity are shown in Fig. 8. Because of symmetry, again, only one-half of the problem geometry is modelled. Both the top surface and the interface are modelled with 15 elements each while four elements are used to discretize the cavity wall. The surface discretization is extended up to a distance of $9a$, where $a = 10$ is the radius of the cavity. The various material properties are as follows:

$$\text{top layer:} \quad \mu_1 = 647{,}200 \quad \nu_1 = 0.35 \quad \rho_1 = 3.25$$

$$\text{half-space:} \quad \mu_2 = 1{,}991{,}150 \quad \nu_2 = 0.30 \quad \rho_2 = 2.85.$$

Figure 9a depicts the time history of the vertical displacements at three selected stations A$(0, 0)$, B$(2a, 0)$ and C$(4a, 0)$ on the free surface. It is observed that the maximum amplitude of vertical disturbance attenuates with distance, as expected. The corresponding results for horizontal displacements at stations B and C are presented in Fig. 9b. It is interesting to note that the maximum horizontal displacement at B is comparable to its vertical disturbance while for point C, the peak horizontal amplitude is quite high as compared to the corresponding vertical displacement.

CONCLUSION

An advanced algorithm for 2D transient dynamics based on direct time-domain boundary element formulation has been used to study a series of problems involving transient wave propagation. Higher order spatial variations (quadratic) as well as temporal variations (linear, mixed) are incorporated for proper modelling and accurate analysis of dynamic problems. Also, simpler and better behaved boundary kernels have been developed and implemented. The problems studied such as transient disturbances due to load applied on the surface of a half-space or layered half-space, vibration isolation using various types of trench and surface disturbance due to an underground explosion demonstrate the ability of the algorithm to handle complicated practical problems.

REFERENCES

Ahmad, S. and Banerjee, P. K. (1988). Multi-domain BEM for two-dimensional problems of elastodynamics. *Int. J. Numer. Meth. Engng* **26**, 891–911.

Antes, H. (1985). A boundary element procedure for transient wave propagation in two-dimensional isotropic elastic media. *Finite Elem. Anal. Des.* **1**, 313–322.

Banerjee, P. K. and Butterfield, R. (1981). *Boundary Element Method in Engineering Science*. McGraw-Hill, London and New York.

Cruse, T. A. and Rizzo, F. J. (1968). A direct formulation and numerical solution of the general transient elastodynamic problem, I. *J. Math. Anal. Appl.* **22**, 244–259.

Graffi, D. (1947). Memorie della Academia Scienze, Bologna Series 10, Vol. 4, pp. 103–109.

Israil, A. S. M. and Banerjee, P. K. (1989). Advanced time-domain formulation of BEM for two-dimensional transient elastodynamics. *Int. J. Numer. Meth. Engng*, to appear.

Lamb, H. (1904). On the propagation of tremors over the surface of an elastic solid. *Phil. Trans. R. Soc. London*, Series **A203**, 1–42.

Mansur, W. J. (1983). A time-stepping technique to solve wave propagation problems using the boundary element method. Ph.D. Thesis, Southampton University.

Niwa, Y., Kobayashi, S. and Azuma, N. (1975). An analysis of transient stresses produced around cavities of arbitrary shape during the passage of travelling wave. *Memo. Fac. Engng Kyoto Univ.* **37**, 28–46.